Optics and Lasers in Engineering 51 (2013) 861–866

Contents lists available at SciVerse ScienceDirect

Optics and Lasers in Engineering

journal homepage: www.elsevier.com/locate/optlaseng

Rapid and accurate extraction of optical parameters for uniaxial bulk media by phase modulated ellipsometry

Chun-I Chuang [a], Shiuan-Huei Lin [b], Yu-Faye Chao [a,*]

[a] Department of Photonics and Institute of Electro-Optical Engineering, National Chiao Tung University, 1001 University Rd., Hsinchu 30010, Taiwan, ROC
[b] Department of Electrophysics, National Chiao Tung University, 1001 University Rd., Hsinchu 30010, Taiwan, ROC

ARTICLE INFO

Article history:
Received 7 August 2012
Received in revised form
28 December 2012
Accepted 2 February 2013
Available online 1 March 2013

Keywords:
Uniaxial
Phase modulated ellipsometry
Genetic algorithm
Refractive index
Orientation of optical axis

ABSTRACT

An improved phase modulated technique has been implemented to increase the speed and accuracy of optical parameters extraction for a uniaxial bulk media. In combination of the genetic algorithm, we show that not only the complex refractive indices, the inclination and azimuth angles of optical axis can also be extracted. Furthermore, by using a two-probe-beam configuration, the speed of convergence can be improved by 5-times. Such a high speed and accurate method can be applied for the in-situ measurement of dynamic materials.

1. Introduction

In the early 1970th, the reflection/transmission coefficients of the anisotropic stratified medium were well investigated [1–3]. The generalized ellipsometry (GE) was introduced to measure the reflection coefficients for deducing the optical parameters (Ops) of an anisotropic medium. Instead of using non-polarized light, researchers [4–8] applied at least three different polarization states to obtain the non-diagonal components of the reflection matrix. In the phase modulated ellipsometry (PME), these polarization states can be rapidly generated by the phase modulator; and the modulated light after interacting with material can be recorded for further analysis [9–15]. For obtaining more Ops of an anisotropic medium, one can increase the number of polarization states to extract the needed Ops. The Ops of an anisotropic medium, such as the uniaxial crystal, in addition to the complex refractive indices, one may have to find the inclination and azimuth angles of the optical axis (OA) with respect to the sample normal and the plane of incidence. The inclination and azimuth angles of OA are usually treated as known in most experiments, in this research, we will use a two-angle of incidence PME to determine all of the Ops of the uniaxial crystal from the acquired intensity waveforms. Because this two-angle of incidence configuration has been performed simultaneously, the determination can be fast and accurate.

There are few numerical processes [16] that have been introduced to retrieve the physical parameters in the multi-parameters inverse problem. Holland [17] based on the mechanism of natural evolution, known as the genetic algorithm (GA), to find the global optimal solution in the complex multi-dimensional search spaces. For the traditional derivative based algorithms, it will be too complicated to compute a large number of parameters from the measured quantities. Since the GA is a direct random search technique by evaluating the fitness function rather than derivation, it can be applied to continuous or discrete problems for optimized solutions. In the process of GA, the mutation operator can re-introduce new information into the population to avoid being trapped in the local optimum. Besides, the GA works with a population of points instead of single point, therefore the optimal solution can be obtained in a relatively short time. The GA has been applied in ellipsometry to determine the refractive indices and thicknesses of multi-layered isotropic media [16,18–21]. By using the inverse genetic algorithm (IGA), Zaghloul et al. [22] proposed a numerical method to extract four Ops of an isotropic thin film-substrate system from only one measurement at single incident angle and wavelength. In addition to this powerful extraction technique, the GA has also been used to optimize the design of a complex instrumentation [23] for searching the Ops. After analyzing the efficiency of convergence, we will show that the two-angle of incidence configuration in PME is the optimized configuration for uniaxial bulk medium.

* Corresponding author. Tel.: +886 3 5712121x56314; fax: +886 3 5735601.
E-mail address: yfchao@mail.nctu.edu.tw (Y.-F. Chao).

0143-8166/$ - see front matter © 2013 Elsevier Ltd. All rights reserved.
http://dx.doi.org/10.1016/j.optlaseng.2013.02.004

Since the Ops can be extracted from one cycle of the recorded two intensity waveforms, which is 20 μs in this PME, one can combine the two-angle of incidence PME and the GA to measure the dynamically changing optical parameters of anisotropic materials [24].

2. Theoretical background

The reflection geometry for a uniaxial crystal and the experimental setup are shown in Fig. 1. In addition to the complex refractive indices, we are interested in measuring the inclination (θ_c) and the azimuth (θ_a) of the OA with respect to the sample normal and plane of incidence. The PME consists of polarizer (P), photoelastic modulator (PEM) and analyzer (A). The transmission axes of P and A are set at -45° and 45°, respectively. The phase of the transmitted light is modulated by photoelastic modulator (PEM) with $\Delta_p=\Delta_0 \sin\omega t$, where Δ_0 and ω are the amplitude and angular frequency of modulation, respectively. The typical modulation frequency of PEM is 50 kHz, therefore, the combination of P and PEM can generate various polarization states within 20 μs for the measurement. For the simultaneous measurements at two incident angles, the probe beam is split into two (Probe 1 and Probe 2) by a beam splitter (BS) after the laser light passes through P and PEM. One beam is directly incident on the sample at an angle θ_{i1}; the other one is reflected from the BS and mirror then incident on the sample at another angle θ_{i2}. The intensity profiles of both probe beams are measured simultaneously and recorded by the data acquisition (DAQ) system. The reflected polarization state, S_{fj}, can be analyzed by the analyzer. The polarization state can be expressed as

$$S_{fj}=M_{A=45^\circ}M_S M_{effj} M_{PEM} S_i \quad j=1,\ 2, \tag{1}$$

where the subscript $j=1, 2$ denotes the two probe beams with the incident angles θ_{ij}; MPEM is the Jones matrix of PEM with horizontal strain axis. M_{eff1} denotes the effective Jones matrix of BS, and M_{eff2} is matrix of the product of BS and mirror. Both matrices are composed of the ellipsometric parameters Ψ_{effj} and Δ_{effj}, which can be measured directly by the modified

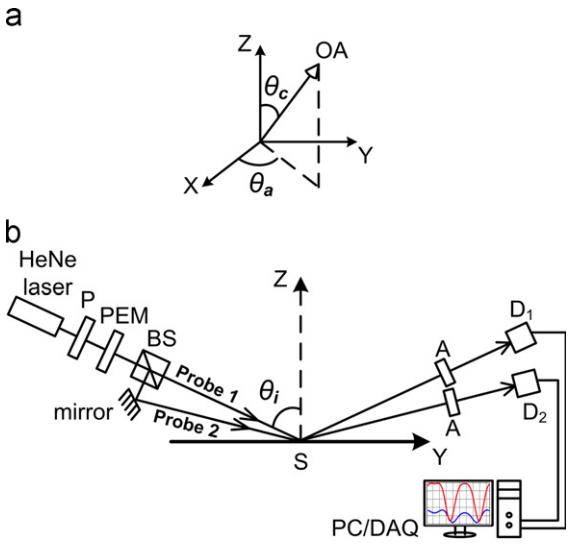

Fig. 1. Two-angle of incidence phase modulated ellipsometer. (a) Geometry of the optical axis of the uniaxial material: optical axis (OA), inclination angle (θ_c), azimuth angle (θ_a). (b) Schematic setup: light source (HeNe laser), polarizer (P), photoelastic modulator (PEM), beam splitter (BS), mirror, two analyzers (A), two photodetectors (D), personal computer (PC) and data acquisition (DAQ) system. The Y–Z plane is the incident plane: incident angle (θ_i), sample (S).

three-intensity measurement technique [25]. MS and $M_{A=45^\circ}$ are the Jones matrices of the sample and analyzer, respectively. The temporal intensity of S_{fj} in Eq. (1) can be expressed as

$$\begin{aligned} I_j(\vec{v},\Delta_p(t)) = I_{0j}[&A - D\cos 2\Psi_{effj} - (B + F\sin 2\Psi_{effj}\sin\Delta_{effj})\cos\Delta_p \\ &+ (C + B\sin 2\Psi_{effj}\sin\Delta_{effj})\sin\Delta_p], \end{aligned} \tag{2}$$

where

$$\begin{aligned} A &= r_{pp,j}(\bar{r}_{pp,j}+\bar{r}_{sp,j}) + r_{ps,j}(\bar{r}_{ps,j}+\bar{r}_{ss,j}) + r_{sp,j}(\bar{r}_{pp,j}+\bar{r}_{sp,j}) + r_{ss,j}(\bar{r}_{ps,j}+\bar{r}_{ss,j}) \\ B &= r_{pp,j}(\bar{r}_{ps,j}+\bar{r}_{ss,j}) + r_{ps,j}(\bar{r}_{pp,j}+\bar{r}_{sp,j}) + r_{sp,j}(\bar{r}_{ps,j}+\bar{r}_{ss,j}) + r_{ss,j}(\bar{r}_{pp,j}+\bar{r}_{sp,j}) \\ C &= i[-r_{pp,j}(\bar{r}_{ps,j}+\bar{r}_{ss,j}) + r_{ps,j}(\bar{r}_{pp,j}+\bar{r}_{sp,j}) - r_{sp,j}(\bar{r}_{ps,j}+\bar{r}_{ss,j}) + r_{ss,j}(\bar{r}_{pp,j}+\bar{r}_{sp,j})] \\ D &= r_{pp,j}(\bar{r}_{pp,j}+\bar{r}_{sp,j}) - r_{ps,j}(\bar{r}_{ps,j}+\bar{r}_{ss,j}) + r_{sp,j}(\bar{r}_{pp,j}+\bar{r}_{sp,j}) - r_{ss,j}(\bar{r}_{ps,j}+\bar{r}_{ss,j}) \\ F &= i[r_{pp,j}(\bar{r}_{ps,j}+\bar{r}_{ss,j}) - r_{ps,j}(\bar{r}_{pp,j}+\bar{r}_{sp,j}) + r_{sp,j}(\bar{r}_{ps,j}+\bar{r}_{ss,j}) - r_{ss,j}(\bar{r}_{pp,j}+\bar{r}_{sp,j})]; \end{aligned} \tag{3}$$

If the subscripts P and S are the polarized light parallel and perpendicular to the incident plane, respectively, then r_{mn}, $(\vec{v})$ is the corresponding Fresnel reflection coefficients for noting its polarization state. The six Ops (n_e, k_e, n_o, k_o, θ_c, θ_a) are noted as $\vec{v}$, which are implicitly contained in the Fresnel reflection coefficients of a uniaxial bulk medium [26–29]. According to Hodgkinson (BTF toolbox) [29], we implemented their program in MATLAB to calculate the Fresnel reflection coefficients of the uniaxial bulk medium. The measured reflected intensities are related to the complex refractive indices and the orientation of the OA of sample. Each parameter has its distinctive effect in the temporal distribution of the reflected intensity profile. Since the variation of reflected intensity is very insensitive to the orientation of OA, we have to separate our fitting procedure into two stages for determining all Ops. In the preliminary stage, the complex refractive indices and normalization intensity (I_0) can be accurately determined because the variations of intensity waveforms are dominated by the complex refractive indices. For obtaining higher precision in θ_c and θ_a, one has to use the predetermined values of complex refractive indices to extract the values of orientation angles by further fitting in GA. Using this waveform extraction technique, we can accurately determine these six Ops by fitting the theoretical intensity profiles to the measured values through GA.

3. Numerical procedure: Analysis and data deduction

In the numerical procedure, the goodness-of-fit can be evaluated by the reduced chi square (RCS) [30,31], which is defined as

$$\mathrm{RCS} = \frac{1}{N-M-1}\sum_{\theta_{ij}}\sum_{t}\frac{(I(\vec{v},\Delta_p(t))_{\mathrm{calc}} - I(\vec{v},\Delta_p(t))_{\mathrm{exp}})^2}{\delta I(\vec{v},\Delta_p(t))^2_{exp}}, \tag{4}$$

where θ_{ij} is the incident angles ($j=1, 2$). One can determine the Ops by optimizing RCS, i.e., RCS ~ 1. The standard deviation of the measurement error $\delta I(\vec{v},\Delta_p(t))_{exp}$ can be determined by repeating the measurements for 100 times [31]. The parameter N is the number of data points, and M is the number of variables. Jellison [30] stated that the fitting results can be a good representation of the experimental data when RCS is approximate to one; while RCS is much larger than one, the fitting results deviate significantly from the experimental data; but if RCS is smaller than one, the error may be overestimated.

The GA sub-functions in MATLAB have been adopted for fitting the theoretical intensity to the measured values. Since the GA is based on the mechanism of natural evolution, the Ops can be labeled as genes in a single chromosome. Each chromosome represents a possible solution of n_e, k_e, n_o, k_o, θ_c, θ_a, and I_{0j} ($j=1$, 2), so there are eight genes (for rwo angles of incidence) in each

chromosome. According to the suggestion of Grefenstette [32], we create 100 chromosomes in a random distribution within the specified boundaries of each gene for its initial population. Using Eq. (4), one can evaluate the chromosomes of the initially generated population then select them into the mating pool according to the rule of roulette wheel. The population of next generation can therefore be generated by crossover and mutation. Since Grefenstette also suggested the probability of crossover and mutation to be 0.25 to 1 and 0 to 0.3, respectively, we choose the probability of crossover and mutation to be 0.8 and 0.08. In this GA data deduction method, the single point crossover and uniform mutation have been selected. To ensure the convergence of this algorithm, the adopted elitist strategy is to compare the performance of two adjacent generations, then preserve the best two chromosomes for the next generation.

3.1. Estimation of complex refractive indices in waveform

The temporal waveform in this PME consists of a very distinguished characteristic for different complex refractive indices ($N=n-i\times k$), which can be used to estimate the complex refractive indices for narrowing down the searching region. First, we concentrate our analysis in the absorbing materials: As the incident angles are at 65 and 70° (these two selected incident angles will be explained later), we set few sets of Ops in Eq. (2) to analyze the normalized intensity distributions, such as shown in Fig. 2(a). The absorbing medium consists of an asymmetric dip in the intensity distribution. The value of averaged extinction coefficient $\overline{k}$ ($\overline{k}=0.5(k_e+k_o)$) and difference Δk ($\Delta k=k_e-k_o$) can be estimated from the height (H) of the dip. The parametric equations, such as Eq. (5), can be obtained by numerical fitting, then it can be plotted in Fig. 2(b). Therefore, not only the averaged extinction coefficient, the values of k_e and k_o can also be estimated by solving the parametric Eq. (5). Since the width (W) of the dip is very hard to estimate because of the discrete property of the temporal phase, we only utilize the height of the dip to estimate the extinction coefficients.

$$\begin{aligned} &H_{70}=p_0+p_1\overline{k}+p_2\overline{k}^2, \quad H_{65}=p_0'+p_1'\overline{k}+p_2'\overline{k}^2\\ &p_0=-0.002+0.003\Delta k, \quad p_0'=-0.006+0.005\Delta k\\ &p_1=0.015-0.021\Delta k, \quad p_1'=0.036-0.042\Delta k\\ &p_2=0.006+0.005\Delta k \quad p_2'=0.003+0.013\Delta k \end{aligned} \tag{5}$$

By analyzing the real part of the complex refractive index (n), one can estimate its values from the minimum value of normalized intensity ($I_{\min}$). In this study, we found that the value of $I_{\min}$ is linearly proportional to the averaged refractive index $\overline{n}$ ($\overline{n}=0.5(n_e+n_o)$), as shown in Fig. 2(c). The parametric equations can be written as $I_{\min}=q_0+q_1\overline{n}$, and the coefficients are linearly proportional to the difference of the refractive indices Δn ($\Delta n=n_e-n_o$). Since this primary estimation is just for providing the initial values in the GA, we only find the parametric equations of $I_{\min}$ versus the refractive indices by assuming $k=0$. Under this concept, the parametric equations are evaluated at the incident angels of 65 and 70°, as Eq. (6). For other extinction coefficients, Eq. (6) can be re-formulated. In the analysis, we also found the orientation of OA has very little effect in temporal waveform.

$$\begin{aligned} &I_{70\min}=q_0+q_1\overline{n}, && I_{65\min}=q_0'+q_1'\overline{n}\\ &q_0=-0.046+0.031\Delta n, && q_0'=-0.056+0.041\Delta n\\ &q_1=0.043-0.022\Delta n, && q_1'=0.060-0.034\Delta n, \end{aligned} \tag{6}$$

3.2. Selection of incident angles

For the optimal design in ellipsometry, we have to analyze the variation of its reflected intensity. In analyzing the derivatives of the reflected intensity profiles with respect to each Op, we realize that the reflected intensity profiles are more sensitive with respect to the variation of each Op at large incident angle. For understanding the efficiency of convergence under different incident angle configurations, population size and mutation rate, we simulate the reflected intensity for a quartz crystal whose OA is orientated at (θ_c, θ_a)=(90°, 90°), then retrieve the Ops by the waveform extraction technique at various conditions. In the analysis, we set the searching range of θ_c and θ_a to be from 0 to 180°; the population size to be 100; and mutation rate to be 0.08. First, we simulate the performance under only one incident angle, for example, 70°. After repeating 100 times of fitting, we obtained 44% unexpected value of θ_c at 53.292 ± 0.004°, which is the local minimum. A similar phenomenon also occurs in determining θ_a. But, we found that one can still extract the Ops as long as one gives large enough population size (>3000 in this PME) and mutation rate (>0.5), which is a time consuming process. Therefore, we study the trapping with respect to the values of population size and mutation rate under different combinations of incident angles. In analyzing the probability of local minimum (PL), within the reasonable population size (100 to 500) and mutation rate (0.08 to 0.3), there is no remarkable improvement in the convergences of

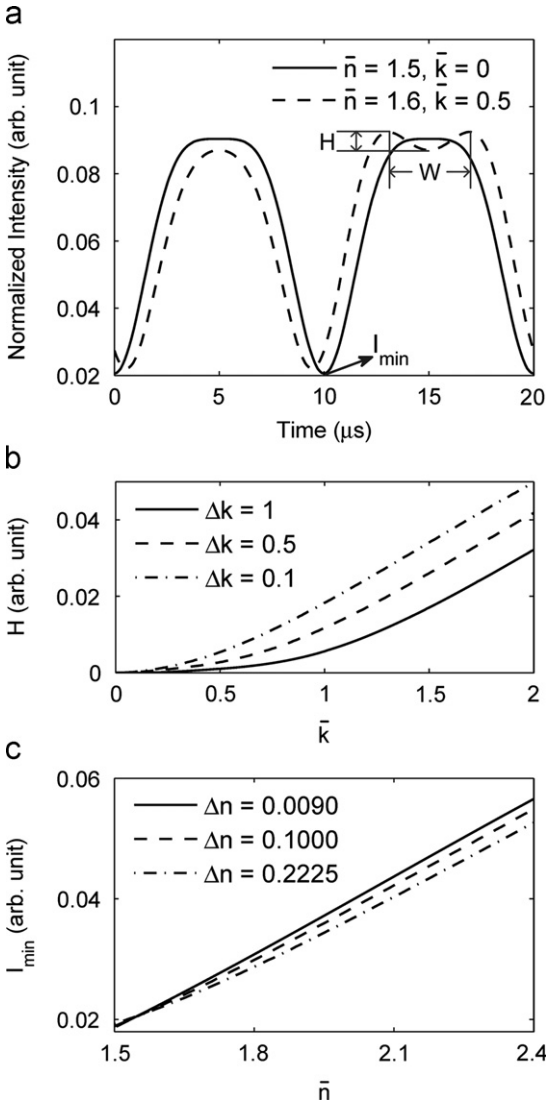

Fig. 2. Estimation for complex refractive index (θ_i=70°): (a) the normalized reflected intensity profile; (b) the parametric equations of the dip depth (H) versus the averaged extinction coefficient; and (c) the parametric equations of the minimum intensity ($I_{\min}$) versus the averaged refractive indices.

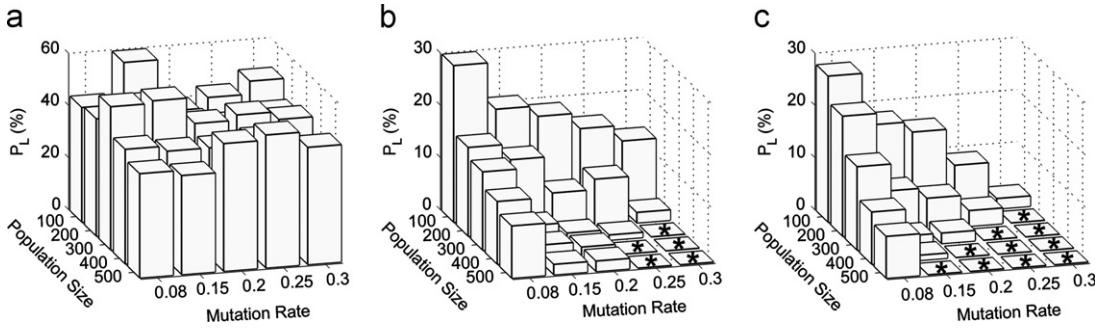

Fig. 3. Probability of local minimum (PL) of θ_c and θ_a at different combinations of incident angles under various GA parameters: (a) single incident angle 70°; (b) two incident angles: 65 and 70°; and (c) three incident angles: 60, 65 and 70°. Asterisks are the zeros.

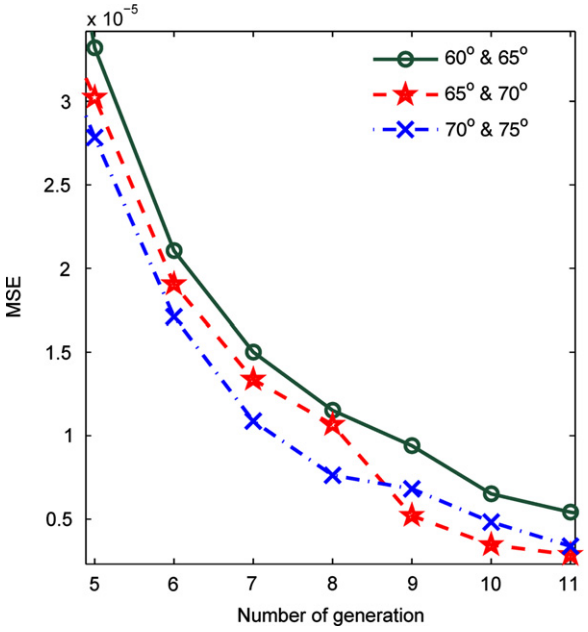

Fig. 4. Convergence of the genetic algorithm for different pair of incident angles: The unbiased estimator (MSE) is plotted against the number of generations in genetic algorithm.

determining θ_c and θ_a by using three incident angles, such as shown in Fig. 3. The computational effort, product of population size and number of generation to convergence [22], can also be useful for estimating the efficiency of convergence. The computational efforts in this waveform extraction technique for the configuration of one-, two- and three-angle of incidence are 53,000, 11,000, and 9300, respectively. From all these considerations and the complexity of the experimental setup, we choose the two-angle of incidence for measuring the Ops of the uniaxial bulk medium.

For further selection of incident angles, we shall analyze the efficiency of convergence for different pairs of incident angles. In this analysis, we use the unbiased estimator (mean squared error, MSE) to evaluate the efficiency of convergence by simulation. By performing 50 generations through a selection–crossover–mutation–elitism loop of GA iterations for three pairs of incident angles, we plot the MSE versus the number of generations in Fig. 4. It is clear to us that 65 and 70° is the best pair for measuring the Ops in PME.

4. Experiments

The schematic setup of the two-angle of incidence PME is shown in Fig. 1(b). The probe beam was a HeNe laser (05LHP171, Melles Griot) at 632.8 nm. The P and A (03FPG015, Melles Griot) were set at $-45°$ and 45° with respect to the incident plane. The polarization state generator consisted of a P and PEM (PEM 90/CF50, Hinds Instruments). As in Ref. [10], we set the modulation amplitude of the PEM to be π, and the azimuth of the strain axis to be 0°. The initial phase of the PEM was calibrated according to Ref. [33]. The intensity of light was measured by the photodetectors (PDA36A, Thorlabs) through the data acquisition system (PCI 6115, National Instruments). Since the modulation frequency of PEM is around 50 kHz and the sampling rate of DAQ card is 10 MS/s per channel, one can acquire 200 data for each cycle ($\sim$20 μs), and therefore, 400 data under 2 incident angles.

Since our job is mainly for probing the photoinduced process of the photopolymer [34], the material under the probing wavelength should exhibit no absorption to interfere the photoinduced process. Three uniaxial media were chosen for verifying the ability of this technique; these media exhibit different anisotropy (Δn) and were cut with different inclination angles: quartz ($\Delta n=0.009$, surface flatness$=\lambda/4$); YVO_4 (CASIX, $\Delta n=0.22$, surface flatness$=2\lambda$) crystals and a c-cut $LiNbO_3$ plate ($\Delta n=-0.084$, thickness$=1$ mm, surface flatness$=\lambda/4$). Their inclination angles θ_c were specified as 90°, 135° and 0°, respectively. For suppressing the multiple reflections of the $LiNbO_3$ plate, we taped the Scotch tape (a translucent adhesive tape) on the back surface of the measurement spot [35]. To examine the application of this PME for a general orientation, we set the azimuthal angle θ_a of quartz and YVO_4 crystals at (1) $90\pm0.01°$ and (2) $0\pm0.01°$, which have been carefully aligned through analytical measurement [25]. Since it is very difficult to align the azimuthal angle when the inclination angle is close to 0°, the $LiNbO_3$ plate has been measured for two complementary azimuth angles by rotating 90° around the sample normal.

The BS and mirror were used to generate two probe beams for simultaneous measurements at two incident angles. However, since both the optical components will alter the polarization states of the incident light, the effective ellipsometric parameters $\Psi_{eff1,2}$ and $\Delta_{eff1,2}$ have been calibrated by the modified three-intensity technique [25].

For understanding the linear dichroism of medium, we simulated the reflected intensity profile from an optical flat $LiNbO_3$ for the probing wavelength to be at 236.2 nm, where one can examine the anisotropy of its refractive indices and extinction coefficients (according to Ref. [36] Ne$=2.98-1.0i$, No$=3.22-1.6i$). Under the incident angles of 65 and 70°, the reflected intensity profiles were simulated at the following four specific OA orientations: (1) $(\theta_c, \theta_a)=(90°, 90°)$; (2) $(\theta_c, \theta_a)=(90°, 0°)$; (3) $\theta_c=0°$; and (4) $(\theta_c, \theta_a)=(5°, 0°)$, where one can analyze the limitation of this technique for measuring the OA orientations.

5. Results and discussion

For the chosen two incident angles, we have calibrated the effective ellipsometric parameters of these two beams. The measured

effective ellipsometric parameters ($\Psi_{eff1,2}$, $\Delta_{eff1,2}$) for the two probe beams are (44.99°, 11.29°) and (43.13°, 56.86°), respectively. After this calibration, we simultaneously measured the crystals at two incident angles to obtain a set of data for optical parameter deduction. The values of the complex refractive indices can be estimated by the parametric functions in Eqs. (5) and (6) for reducing the GA searching ranges. The measured dip height was around 10–5 for these three crystals, so the anisotropic absorption is too low to be resolved in this technique (k_e and k_o are reduced to one parameter, k). By assuming a flat interface between the ambient and the bulk material [37,38], the pseudo-refractive indices and the orientation angles can be obtained after two fitting stages, then we list the results in Table 1. The main task of this work is to calibrate this technique, two probe beams, so the system errors are compared with the known values, such as the Ops of quartz crystal and YVO_4, both of which have been studied [39] by other method. According to the rule of thumb [40] in statistics, we obtain random errors by 50 fittings of GA. The intensity profiles measured within 20 μs and the calculated ones are compared in Fig. 5, where only 1/5 of the measured data are displayed for a clear vision. Furthermore, the surface roughness is also analyzed and modeled using the Bruggeman effective medium approximation [41], consisting of 50% void and 50% material. In this analysis, the thickness of the overlayer for these three materials is obtained as less than 1 nm. The resultant Ops of the materials deviate less than 0.1% from the refractive indices and less than 1% from the orientation angles in Table 1. Therefore, the overlayer can be neglected here under $\lambda=632.8$ nm. The refractive indices determined by this system for these selected samples are comparable to the known values [42]. Although the quartz crystal does exhibit optical activity, its influence on the refractive index ellipsoid is too small to be detected (according to Ref. [43], the radius distortion is from $\pm 2.7\times10^{-8}$ to $\pm 2.4\times10^{-5}$, depending on the angle between the direction of propagating light and OA). It is clear that one can determine the orientation angles of YVO_4 with higher precisions than that of quartz crystal, which is due to the larger difference between ne and no. The inclination angle θ_c of YVO_4 specified as by the vendor (CASIX) is 135°. According to the measurement of this PME, θ_c is 136.006 ± 0.004°, which is comparable to our previous measurements [39]. For $LiNbO_3$, θ_c measured by this technique is approximately 178° instead of the specified value as

Table 1
Optical parameters of Quartz, YVO_4 and $LiNbO_3$ crystals: determined from the measured waveforms of the two angles of incidence PME.

Quartz	n_e	n_o	k	θ_c	θ_a	RCS
1	1.553 ± 0.001	1.544 ± 0.002	0.0001 ± 0.0001	90.01 ± 0.01°	$89.99\pm\pm0.02$°	1.05
2	1.553 ± 0.003	1.543 ± 0.002	0.0001 ± 0.0001	89.8 ± 0.1°	0.04 ± 0.02°	1.49
Referred value [a]	1.552	1.543	–	–	–	
YVO_4						
1	2.215 ± 0.003	1.994 ± 0.003	0.002 ± 0.004	136.006 ± 0.004°	89.992 ± 0.006°	1.39
2	2.216 ± 0.003	1.993 ± 0.003	0.0002 ± 0.0002	135.974 ± 0.002°	0.056 ± 0.004°	1.26
Referred value [a]	2.216	1.996	–	–	–	
$LiNbO_3$						
1	2.201 ± 0.002	2.285 ± 0.001	0.0010 ± 0.0004	178.4 ± 0.1°	–	1.51
2	2.201 ± 0.003	2.283 ± 0.001	0.0012 ± 0.0002	178.1 ± 0.1°	–	1.62
Referred value [a]	2.202	2.286	–	–	–	

[a] Ref. [42].

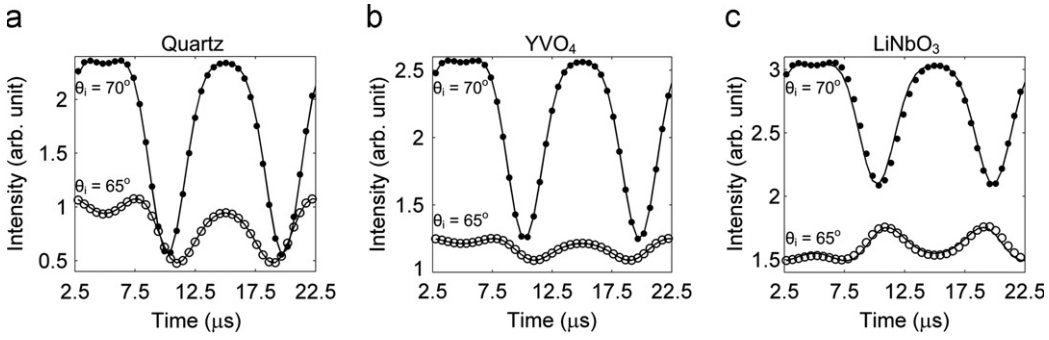

Fig. 5. Measured reflected intensity profiles at incident angles of 65° (○) and 70° (●): (a) quartz, (b) YVO_4 and (c) $LiNbO_3$. All these measured value are compared with the calculated values (–). Only 1/5 data points in each cycle are displayed for case 1.

Table 2
Optical parameters of $LiNbO_3$ crystal: determined from the simulated waveform.[a]

$LiNbO_3$ (θ_c, θ_a)	n_e	k_e	n_o	k_o	θ_c	θ_a
1 (90°, 90°)	2.9752 ± 0.0001	1.0028 ± 0.0003	3.2150 ± 0.0001	1.5957 ± 0.0001	89.98 ± 0.01°	90.03 ± 0.01°
2 (90°, 0°)	2.9803 ± 0.0002	1.0000 ± 0.0002	3.220 ± 0.003	1.600 ± 0.002	90.08 ± 0.04°	0.01 ± 0.01°
3 (0°, N/A)	2.983 ± 0.001	1.0019 ± 0.0001	3.2248 ± 0.0002	1.6022 ± 0.0001	178.85 ± 0.02°	–
4 (5°, 0°)	2.982 ± 0.003	1.0015 ± 0.0003	3.2200 ± 0.0002	1.6011 ± 0.0002	5.32 ± 0.03°	0.61 ± 0.06°
Referred value [b]	2.98	1.0	3.22	1.6	–	–

[a] The results were obtained by repeating the fitting process for 50 times.
[b] Ref. [36].

0/180°. This means we cannot determine the orientation of OA of a uniaxial medium when its OA is perpendicular to the sample surface.

For verifying the validity of this technique, we perform a computational experiment (the specific condition are stated in the experiment) by simulating the reflected waveform of $LiNbO_3$ then extract its Ops from the simulated waveforms while its OA are at four different orientations. The determined Ops listed in Table 2 show that the complex refractive indices can be accurately determined at any orientation of OA, but θ_c and θ_a can be determined only when the OA is inclined more than 5° off-normal, which is the limitation of this technique.

6. Conclusions

In this research, we have established a rapid and accurate method to measure the Ops of uniaxial crystals by using two probe beams, simultaneously. Through the numerical analysis, we not only suggest the appropriate incident angle pair to measure the complex refractive indices and OA directions, we also provide the appropriate initial boundaries for reducing the computation time in GA. Although, we did not measure any absorbing material, the anisotropic complex refractive indices and orientation of its OA have been examined through the computational experiment of $LiNbO_3$ at 236.2 nm. The analysis indicates that this two-angle of incidence PME can measure the complex refractive indices of a uniaxial crystal when its OA is oriented in any direction, but can determine its direction only when the OA is orientated more than 5° off-normal. In combination of the two-angle of incidence PME and the GA, one can extract the Ops from the intensity waveforms recorded within 20 μs, therefore, this technique can be applied for the dynamic in-situ measurement of the anisotropic medium.

Acknowledgement

Authors acknowledge the funding from the National Science Council of Taiwan under grant number NSC98-2221-E-009-024. We also appreciate Dr. Ian J. Hodgkinson for his help in the implement of BTF toolbox program.

References

[1] Teitler S, Henvis BW. Refraction in stratified, anisotropic media. J Opt Soc Am 1970;60:830–4.
[2] Berreman DW. Optics in stratified and anisotropic media: 4×4-matrix formulation. J Opt Soc Am 1972;62:502–10.
[3] Azzam RMA, Bashara NM. Ellipsometric measurement of the polarization transfer function of an optical system. J Opt Soc Am 1972;62:336–40.
[4] Azzam RMA, Bashara NM. Application of generalized ellipsometry to anisotropic crystals. J Opt Soc Am 1974;64:128–33.
[5] Alonso MI, Garriga M, Alsina F, Piñol S. Determination of the dielectric tensor in anisotropic materials. Appl Phys Lett 1995;67:596–8.
[6] Schubert M, Rheinländer B, Woollam JA, Johs B, Herzinger CM. Extension of rotating-analyzer ellipsometry to generalized ellipsometry: determination of the dielectric function tensor from uniaxial TiO_2. J Opt Soc Am A 1996;13:875–83.
[7] Hodgkinson I, Hazel J, Wu QH. In situ measurement of principal refractive indices of thin films by two-angle ellipsometry. Thin Solid Films 1998; 313-314:368–72.
[8] Beaudry NA, Zhao Y, Chipman R. Dielectric tensor measurement from a single Mueller matrix image. J Opt Soc Am A 2007;24:814–24.
[9] Jellison Jr GE, Modine FA, Boatner LA. Measurement of the optical functions of uniaxial materials by two-modulator generalized ellipsometry: rutile (TiO_2). Opt Lett 1997;22:1808–10.
[10] Wang MW, Chao YF, Leou KC, Tsai FH, Lin TL, Chen SS, et al. Calibrations of phase modulation amplitude of photoelastic modulator. Jpn J Appl Phys 2004;43:827–32.
[11] Han CY, Chao YF. Photoelastic modulated imaging ellipsometry by stroboscopic illumination technique. Rev Sci Instrum 2006;77:023107.
[12] Yu TC, Lo YL. A novel heterodyne polarimeter for the multiple-parameter measurements of twisted nematic liquid crystal cell using a genetic algorithm approach. J Lightwave Technol 2007;25:946–51.
[13] Diner DJ, Davis A, Hancock B, Gutt G, Chipman RA, Cairns B. Dual-photoelastic-modulator-based polarimetric imaging concept for aerosol remote sensing. Appl Opt 2007;46:8428–45.
[14] Petkovšek R, Bammer F, Schuöcker D, Možina J. Dual-mode single-crystal photoelastic modulator and possible applications. Appl Opt 2009;48:C86–91.
[15] Martínez-Ponce G, Solano C, Pérez-Barrios C. Hybrid complete Mueller polarimeter based on phase modulators. Opt Lasers Eng 2011;49:723–8.
[16] Polgár O, Fried M, Lohner T, Bársony I. A combined topographical search strategy with ellipsometric application. J Global Optim 2001;19:383–401.
[17] Holland JH. Adaptation in natural and artificial systems. Ann Arbor, MI: University of Michigan Press; 1975 pp. 183.
[18] Fernandes VR, Vicente CMS, Wada N, André PS, Ferreira RAS. Multi-objective genetic algorithm applied to spectroscopic ellipsometry of organic-inorganic hybrid planar waveguides. Opt Express 2010;18:16580–6.
[19] Cormier G, Boudreau R. Genetic algorithm for ellipsometric data inversion of absorbing layers. J Opt Soc Am A 2000;17:129–34.
[20] Kudla A. Application of the genetic algorithms in spectroscopic ellipsometry. Thin Solid Films 2004;455–456:804–8.
[21] Cardin J, Leduc D. Determination of refractive index, thickness, and the optical losses of thin films from prism-film coupling measurements. Appl Opt 2008;47:894–900.
[22] Zaghloul YA, Zaghloul ARM. Single-angle-of-incidence ellipsometry. Appl Opt 2008;47:4579–88.
[23] Hölzel R, Bentley PM, Fouquet P. Instrument design and optimization using genetic algorithms. Rev Sci Instrum 2006;77:105107.
[24] Chuang CI, Lin SH, Chao YF. Opt Mater 2013;35:366–71.
[25] Chao YF, Lee KY, Lin YD. Analytical solutions of the azimuthal deviation of a polarizer and an analyzer by polarizer-sample-analyzer ellipsometry. Appl Opt 2006;45:3935–9.
[26] Schubert M. Polarization-dependent optical parameters of arbitrarily anisotropic homogeneous layered systems. Phys Rev B: Condens Matter 1996;53: 4265–74.
[27] Jellison GE, Modine FA. Two-modulator generalized ellipsometry: theory. Appl Opt 1997;36:8190–8.
[28] Lekner J. Reflection ellipsometry of uniaxial crystals. J Opt Soc Am A 1997;14:1359–62.
[29] Hodgkinson IJ, Wu QH. Birefringent thin films and polarizing elements. Singapore: World Scientific; 1997.
[30] Jellison Jr GE. Use of the biased estimator in the interpretation of spectroscopic ellipsometry data. Appl Opt 1991;30:3354–60.
[31] Laub CF, Kuhl TL. Fitting a free-form scattering length density profile to reflectivity data using temperature-proportional quenching. J Chem Phys 2006;125:244702.
[32] Grefenstette JJ. Optimization of control parameters for genetic algorithms. IEEE Trans Syst Man Cybern SMC-16 1986:122–8.
[33] Tsai HM, Chen LC, Chao YF. Ultra fast self-corrected polarization modulated ellipsometer. Thin Solid Films 2011;519:2746–9.
[34] Sekkat Z, Wood J, Knoll W. J Phys Chem 1995;99:17226–34.
[35] Synowicki RA. Suppression of backside reflections from transparent substrates. Phys Stat Sol (c) 2008;5:1085–8.
[36] Palik ED. Lithium niobate ($LiNbO_3$). In: Palik ED, editor. Handbook of optical constants of solids, vol. 1. Orlando: Academic Press; 1985. p. 699.
[37] Jellison Jr GE, Baba JS. Pseudodielectric functions of uniaxial materials in certain symmetry directions. J Opt Soc Am A 2006;23:468–75.
[38] Fujiwara H. Spectroscopic ellipsometry: principles and applications. qChichester: Wiley; 2007 pp. 147–248.
[39] Chao YF, Wang MW, Ko ZC. An error evaluation technique for the angle of incidence in a rotating element ellipsometer using a quartz crystal. J Phys D: Appl Phys 1999;32:2246–9.
[40] Hill T, Lewicki P. Statistics: methods and applications: a comprehensive reference for science, industry, and data mining. Stat Soft, Tulsa 2006:19.
[41] Bruggeman DAG. Berechnung verschiedener physikalischer konstanten von heterogenen substanzen. I. dielektrizitätskonstanten und leitfähigkeiten der mischkörper aus isotropen substanzen. Ann Phys 1935;416:636–79.
[42] Tropf WJ, Thomas ME, Rogala EW. Properties of crystals and glasses. In: third ed. Bass M, editor. Handbook of optics, vol. 4. New York: McGraw–Hill; 2009. p. 2.63–5.
[43] Nye JF. Physical properties of crystals. Oxford: Oxford University Press; 1985 pp. 263.